

SI Appendix

Methods

Synthesis of Pyr3. A mixture of ethyl 2-(ethoxymethylene)-4,4,4-trifluoro-3-oxo-butyrate (4.80 g, 20.0 mmol), 4-nitrophenylhydrazine (3.06 g, 20.0 mmol), and H₂SO₄ (0.5 ml) in EtOH (50 ml) was refluxed overnight. After cooling to room temperature, red-brown solid was precipitated, and the solid was obtained by filtration. After drying *in vacuo*, red-brown solid **1** was obtained. Yield: 5.37 g (82%). ¹H-NMR (400 MHz, CDCl₃) δ/ppm 8.39 (dd, 2H, J = 8.8, 2.0 Hz), 8.17 (s, 1H), 7.66 (d, 2H, J = 8.8 Hz), 4.40 (q, 2H, J = 7.0 Hz), 1.40 (t, 3H, J = 7.0 Hz).

Five% Pd-C was added to a reaction mixture of **1** (1.00 g, 3.05 mmol) in ethyl acetate (10 ml), and stirred for 2 h at room temperature under H₂ atmosphere. After removal of Pd-C by filtration, the solvent was evaporated. After drying *in vacuo*, red-brown solid **2** was obtained. Yield: 0.89 g (87%). ¹H-NMR (400 MHz, CDCl₃) δ/ppm 8.06 (s, 1H), 7.17(d, 2H, J = 8.8 Hz), 6.71(d, 2H, J = 8.8 Hz), 4.36(q, 2H, J = 7.2 Hz), 3.92(s, 2H), 1.38(t, 3H, J = 7.2 Hz).

A mixture of **2** (0.127 g, 0.424 mmol), 2,3,3-trichloro-acrylic acid (0.126 g, 0.718 mmol), (benzotriazol-1-yloxy)tris(dimethylamino)phosphonium hexafluorophosphate (BOP) (0.653 g, 1.27 mmol), and N,N-diisopropylethylamine (DIEA) (0.296 ml, 1.70 mmol) in dry dimethylformamide (DMF) 10 ml was stirred overnight at room temperature. After removal of the solvent, ethyl acetate was added to the residue. After washing with citric acid solution and brine, the organic layer was dried over MgSO₄. The residue was purified by column chromatography (silica, hexane : ethyl acetate = 6 : 1 → 5 : 2). After drying *in vacuo*, white solid (Pyr3) was obtained.

Yield: 68.4 mg (35%). ¹H-NMR (400 MHz, CDCl₃) δ/ppm 8.11(s, 1H), 7.99 (s, 1H), 7.73 (d, 2H, J = 8.8 Hz), 7.44 (d, 2H, J = 8.8 Hz), 4.38 (q, 2H, J = 7.2 Hz), 1.39 (t, 3H, J = 7.2 Hz).

Synthesis of Pyr4. A mixture of 4-Methyl-[1,2,3]thiadiazole-5-carboxylic acid (71 mg, 0.49 mmol) and thionyl chloride (0.51 ml, 7.6 mmol) in dry THF (4 ml) was stirred overnight at 60°C. After removal solvent and drying in vacuo, a mixture of the residue, **2** (102 mg, 0.341 mmol), and DIEA (170 μl, 0.98 mmol) in CH₂Cl₂ (3 ml) was stirred for 2 h at room temperature. After removal of the solvent, ethyl acetate was added to the residue. After washing with 0.1N HCl and brine, the organic layer was dried over MgSO₄. The residue was purified by column chromatography (silica, hexane : ethyl acetate = 2 : 1). After drying *in vacuo*, yellow solid (Pyr4) was obtained. Yield: 96.6 mg (61%). ¹H- NMR (400 MHz, CDCl₃) δ/ppm 8.12 (s, 1H), 7.76 (d, 2H, J = 8.8 Hz), 7.61 (s, 1H), 7.47 (d, 2H, J = 8.8 Hz), 4.38 (q, 2H, J = 7.2 Hz), 3.00 (s, 3H), 1.39 (t, 3H, J = 7.2 Hz).

Synthesis of Pyr5. A mixture of 1,1,1,5,5,5-hexafluoro-2,4-pentanedione (4.80 g, 17.0 mmol), 4-nitrophenylhydrazine (2.60 g, 20.0 mmol), and H₂SO₄ (0.5 ml) in EtOH (40 ml) was refluxed overnight. The reaction mixture was neutralized with saturated NaHCO₃ solution, and extracted with CHCl₃. The residue was purified by column chromatography (silica, hexane : ethyl acetate = 8 : 1) to obtain a yellow-brown liquid **4**. Yield: 2.17 g (39%). ¹H-NMR (400 MHz, CDCl₃) δ/ppm 8.43-8.40 (m, 2H), 7.78-7.74 (m, 2H), 7.17(s, 1H).

Five% Pd-C was added to a reaction mixture of **4** (1.04 g, 3.21 mmol) in ethyl acetate

(10 ml), and stirred for 2 h at room temperature under H₂ atmosphere. After removal of Pd-C by filtration, the solvent was evaporated. After drying *in vacuo*, red-brown solid **5** was obtained. ¹H-NMR (400 MHz, CDCl₃) δ/ppm 7.24-7.22 (m, 2H), 7.00 (s, 1H), 6.74-6.71 (m, 2H), 3.93 (s, 2H).

A mixture of 2,3,3-trichloro-acrylic acid (0.184 g, 1.05 mmol) and thionyl chloride (0.60 ml, 8.9 mmol) in dry THF (4 ml) was stirred 2.5 h at 60°C. After removal of solvent and drying *in vacuo*, a mixture of the residue, **5** (0.212 g, 0.718 mmol), and DIEA (366 μl, 2.10 mmol) in dry CH₂Cl₂ (4 ml) was stirred overnight at room temperature. After removal of the solvent, ethyl acetate was added to the residue. After washing with 0.1N HCl and brine, the organic layer was dried over MgSO₄. The residue was purified by column chromatography (silica, hexane : ethyl acetate = 6 : 1). After drying *in vacuo*, yellow solid (Pyr5) was obtained. Yield: 0.100 mg (31%). ¹H- NMR (400 MHz, CDCl₃) δ/ppm 7.94 (s, 1H), 7.75 (m, 2H), 7.52 (m, 2H), 7.07 (s, 1H).

Synthesis of Pyr-PP. In a round bottom flask, **7** (198 mg, 0.76 mmol) and K₂CO₃ 700mg (38.1 mmol) were suspended in 25 ml dry THF, then bromoacetone 194 μl (22.8 mmol) was added. After stirring for 3 h at room temperature, the solvent was removed. The organic layer was washed with brine, and dried over MgSO₄. The residue was purified by column chromatography (silica, hexane : ethyl acetate = 4 : 1→2 : 1). After drying *in vacuo*, yellow solid **8** was obtained. Yield: 226 mg (94%). ¹H- NMR (400 MHz, CDCl₃) δ/ppm 7.54 (m, 1H), 7.46 (s, 1H), 7.00 (s, 1H), 4.63 (s, 2H), 3.92 (s, 3H), 2.35 (s, 3H).

In a round bottom flask, **8** (122 mg, 0.39 mmol) was dissolved in 17 ml methanol, then

1N LiOH aqueous solution 6.8 ml was added. After stirring for 1 h at 4°C, 10% citric acid solution was added for neutralization. After removal of methanol, the solution was acidified to pH2~3, and CH₂Cl₂ were added for extraction. White solid **9** was obtained after drying *in vacuo*. Yield: 120 mg (100%). ¹H-NMR (400 MHz, CDCl₃) δ/ppm 7.57 (m, 1H), 7.54 (s, 1H), 7.04 (s, 1H), 4.65 (s, 2H), 2.31 (s, 3H).

In a round bottom flask, **9** (50 mg, 0.17 mmol) was dissolved in 1.5 ml of dry CH₂Cl₂, and then thionyl chloride 26 μl was added. After refluxing for 3 h, solvent was removed to obtain oiled compound **10**. Then, 102 mg (0.341 mmol) of **5**, 170 μl (0.98 mmol) of DIEA, and 3 ml of dry CH₂Cl₂ were added to the flask under N₂ atmosphere. The reaction mixture was stirred for 2 h at room temperature, and then diluted with ethyl acetate. The organic layer was washed with 1N HCl and saturated NaHCO₃ solution and brine, and dried over MgSO₄. After removal of MgSO₄, the solvent was evaporated. The residue was purified by flash column chromatography (silica). After drying *in vacuo*, yellow solid (Pyr-PP) was obtained. Yield: 46 mg (48%). FAB-Mass *m/z* 780 [(M+H)⁺].

Cell Culture and cDNA Expression. HEK293 cells or HEK293T cells were cultured in Dulbecco's modified Eagle's medium (DMEM) containing 10% fetal bovine serum, 30 units/ml penicillin, and 30 μg/ml streptomycin. Cells were co-transfected with pCI-neo-mouseTRPC1α, pCI-neo-mouseTRPC2, pCI-neo-mouseTRPC3, pCI-neo-mouseTRPC4β, pCI-neo-mouseTRPC5, pCI-neo-mouseTRPC6, pCI-neo-mouseTRPC7, or pCI-neo-mouseTRPM4b and pEGFP-F (Clontech) as a marker. Transfection was carried out using SuperFect Transfection Reagent (Qiagen) for HEK293 cells or Lipofectamine 2000 (Invitrogen) for HEK293T cells according to

manufacturer's instructions. DT40 cell culture and cDNA expression of rat PLC γ 2-EYFP in DT40 cells were performed as described previously (1).

Measurement of Changes in $[Ca^{2+}]_i$. The fura-2 fluorescence images of the cells were recorded in the HEPES-buffered saline (HBS) (in mM): 107 NaCl, 6 KCl, 1.2 MgSO $_4$, 2 CaCl $_2$, 1.2 KH $_2$ PO $_4$, 11.5 glucose, 20 HEPES (pH 7.4 adjusted with NaOH) in HEK293 cells, or the physiological salt solution (PSS) (in mM): 150 NaCl, 8 KCl, 1 MgCl $_2$, 2 CaCl $_2$, 5 HEPES, 5.6 glucose (pH 7.4 adjusted with NaOH) in DT40 cells as previously reported (1). Ca $^{2+}$ -free solution contains 0.5 mM EGTA but no added CaCl $_2$. The fluorescent images were analyzed with a video image analysis system (AQUACOSMOS, Hamamatsu Photonics). All the reagents dissolved in water or dimethylsulfoxide were diluted to their final concentrations, and applied to the cells by perfusion. IC $_{50}$ values were determined by using KaleidaGraph (Synergy Software). Initial rate ($d[Ca^{2+}]_i/dt$) of Ca $^{2+}$ influx was determined by linear fitting of measured $[Ca^{2+}]_i$ data points over the first 60 s after readministration of 2 mM Ca $^{2+}$ to the extracellular solution under stimulation of the receptors.

Electrophysiology. Whole-cell mode of the patch-clamp technique was performed on HEK293 or HEK293T cells at room temperature (22–25°C) with an EPC-9 (HEKA, Darmstadt) or Axopatch 200B (Axon Instruments, Union City, CA) patch-clamp amplifier as previously described (2). Voltage-clamp experiments were performed at a holding potential of –50 mV or –60 mV, and recordings were sampled at 2.0 kHz and filtered at 2.9 kHz. The I - V relationships were determined using a 50-, 200-, or 400-ms voltage ramp from –100 mV to +100 mV or from –120 mV to +80 mV.

Pipette resistance ranged from 2 to 6 megohm when filled with the pipette solution described below. The series resistance was electronically compensated to > 50%. An external solution contained (in mM): For TRPC3 and C6, 140 NaCl, 5 KCl, 2 CaCl₂, 1 MgCl₂, 10 glucose, 10 HEPES (pH 7.4 adjusted with NaOH). For TRPM4b, 110 NaCl, 5 CaCl₂, 10 glucose, 10 HEPES (pH 7.4 adjusted with NaOH). The pipette solution contained (in mM): For mAChR-activated TRPC3 current, 95 CsOH, 95 aspartate, 40 CsCl, 4 MgCl₂, 5 EGTA, 2 ATPNa₂, 5 HEPES, 8 creatine phosphate (pH 7.2 adjusted with CsOH). For OAG-induced TRPC3 current, 130 CsOH, 130 glutamate, 3.1 MgCl₂, 2.8 CaCl₂, 10 EGTA, 2 ATPNa₂, 0.3 GTPNa₂, 10 HEPES (pH 7.2 adjusted with CsOH). For TRPC6 current, 145 CsOH, 145 aspartate, 2 MgCl₂, 0.3 CaCl₂, 10 EGTA, 10 HEPES (pH 7.2 adjusted with CsOH). For TRPM4b current, 110 CsOH, 110 aspartate, 4 MgCl₂, 8.4 CaCl₂, 10 EGTA, 4 ATPNa₂, 10 HEPES (pH 7.4 adjusted with CsOH). The osmolarity of the external solutions was adjusted to about 300 mOSM. No significant difference ($P = 0.74$) was observed in membrane capacitance between the control (22.7 ± 2.4 pF) and Pyr3-treated (21.2 ± 2.5 pF) HEK293 cells expressing TRPC3.

Post-photoaffinity Labeling Modification (P-PALM) and Western Blot Analysis.

The photoaffinity labeling reagent (Pyr-PP) was designed and synthesized (Figure S1E in *SI Appendix*). TRPC3-GFP- or TRPC3-expressing HEK293 cells ($\sim 2 \times 10^6$) were treated with 100 μ M Pyr-PP in HBS solution, and photo-labeling was carried out by UV light irradiation (365 nm) at room temperature (22–25°C) for 30 min. The cells were washed four times with HBS solution and reacted with a 1.5 mM Aldehyde Reactive Probe (ARP) (Dojindo) at 37°C for 1 h. The cells were washed six times with HBS

solution, then lysed with RIPA buffer (pH 8.0) contained: 0.1% SDS, 0.5% sodium deoxycholate, 1% Nonidet P40, 150 mM NaCl, 50 mM Tris-HCl, 1 mM PMSF, and 10 µg/ml leupeptin. In the detection of Pyr-PP-bound TRPC3-GFP protein, Pyr-PP-bound proteins were pull-downed from the cell lysates with 30 µl bed volume of Immobilized NeutrAvidin Protein Plus (PIERCE) at 4°C for 2 h. The beads were washed with the RIPA buffer, and proteins were eluted in SDS sample buffer. The proteins were fractionated by 10% SDS-PAGE and electrotransferred onto a nitrocellulose membrane. The blots were incubated with anti-GFP antibody (Clontech), and detected using the ECL system (Amersahm Pharmacia). In the detection of TRPC3 protein-bound Pyr-PP, TRPC3 protein was immunoprecipitated from the cell lysates with 2 µg anti-TRPC3 antibody (1) at 4°C for 2 h in the presence of 30 µl bed volume of protein A Sepharose (Amersahm Pharmacia). The beads were washed with the RIPA buffer, and proteins were eluted in SDS sample buffer. The proteins were analyzed by western blotting using anti-biotin antibody (Jackson ImmunoResearch Laboratories) and the ECL system.

Electron Microscopic Analysis of Photo-labeled TRPC3. For direct observation of Pyr-PP and TRPC3 complex by electron microscopy, FLAG-tagged TRPC3 protein was used (3). HEK293 cells expressing TRPC3-FLAG ($\sim 5 \times 10^6$) were labeled with 100 µM Pyr-PP and solubilized from the plasma membrane by homogenizing the cells in 500 µl TBS containing 50 mM n-dodecyl-β-D-maltoside (DDM) (Sigma), 0.02% sodium azide and protease inhibitors. After centrifuging for 30 min at $100,000 \times g$, the supernatant was mixed with 20 µl bed volume of an anti-FLAG affinity gel (Sigma). The mixture was incubated at 4°C for 1 h. After washing the gel with 400 µl wash

buffer (TBS containing 5 mM DDM, 350 mM MgCl₂, 0.02% sodium azide), 4 µl of streptavidin-gold conjugate (BBInternational) was added to the mixture and mixed at 4°C for 20 min. Unbound streptavidin-golds were removed by washing the gel with 400 µl wash buffer twice. The TRPC3-Pyr-PP-streptavidin gold complex was eluted from the gel with 40 µl of 100 µg/ml FLAG peptide (Sigma).

The eluate containing gold labeled TRPC3 was adsorbed by thin carbon films supported by copper mesh grids, which were rendered hydrophilic in advance by glow-discharge in low air pressure. Samples were washed with five drops of double-distilled water, negatively stained with 2% uranyl acetate solution for 30 s twice, blotted, and dried in air. Samples were observed by the electron microscopy. Micrographs of negatively stained particles were recorded in a JEOL 100CX transmission electron microscope (JEOL) at × 41,000 magnification with 100 kV acceleration voltages. Images were recorded on SO-163 image films (Eastman Kodak), developed with a D19 developer (Eastman Kodak), and digitized with a Scitex Leafscan 45 scanner (Leaf systems) at a pixel size of 2.44 Å at the specimen level.

Confocal Microscopy and Image Analysis. PLCγ2-EYFP-expressing DT40 cells were plated onto poly-L-lysine coated glass coverslips. Fluorescence images were acquired with a confocal laser-scanning microscope (FV500; Olympus) using the 488-nm line of an argon laser for excitation and a 505-nm to 525-nm band-pass filter for emission. The specimens were viewed at high magnification using Plan oil objectives (60 ×, 1.40 NA; Olympus).

Analysis of ERK Activity. A total of 2.5×10^6 DT40 cells were stimulated with 10

$\mu\text{g/ml}$ anti-IgM in serum-free PSS, and then lysed in 50 μl of lysis buffer (50 mM Tris-HCl pH 7.5, 150 mM NaCl, 5 mM EDTA, 1% Triton X-100, 100 μM Na_3VO_4 , 2 mM dithiothreitol, 2 mM phenylmethylsulfonyl fluoride, 10 $\mu\text{g/ml}$ leupeptin and 5 $\mu\text{g/ml}$ aprotinin) for 10 min on ice. After centrifugation at $10,000 \times g$ for 10 min, the total amounts of protein were quantified using a BCA assay kit (Pierce). Lysates (30 μg total protein) were subjected to 10% SDS-PAGE and electrotransferred onto a nitrocellulose membrane. Activation of ERK was determined by western blotting with anti-phosphospecific p44/p42 (ERK) antibody (Cell Signaling Technology). The total amount of ERK was detected by using anti-ERK2 polyclonal antibody (Santa Cruz Biotechnology). The blots were visualized using the ECL system.

Measurement of Cardiac Hypertrophy *in Vitro* and *in Vivo*. Measurement of NFAT activity and hypertrophic growth of cardiomyocytes was performed as described (4). Briefly, neonatal rat cardiomyocytes were isolated from 1–2 day-old Sprague-Dawley rats, and cultured on the gelatin-coated dishes or laminin-coated silicon rubber dishes. The cDNAs (pNFAT-Luc, pBNP-Luc and pRL-SV40) were transfected by Fugene 6 (Roche) and a recombinant adenovirus encoding GFP-fused amino terminal region of NFAT4 isoform was infected at 100 MOI in serum-free medium. Forty-eight h after transfection, cells were stimulated with Ang II (100 nM) or mechanical stretch by 20%. Cells were treated with Pyr2 or Pyr3 for 20 min prior to the stimulation with Ang II or mechanical stretch. The cells were washed, fixed, and then stained with Alexa Fluor 594-phalloidin to visualize actin filaments. Protein synthesis was measured by [^3H]leucine incorporation. Cells were treated with Pyr2 or Pyr3 for 20 min prior to the stimulation with Ang II (100 nM), and [^3H]leucine (1

$\mu\text{Ci/ml}$) was added to the culture medium and further incubated for 6 h. The incorporated [^3H]leucine was measured using liquid-scintillation counter. IC_{50} values were determined by using GraphPad Prism (GraphPad Software).

TAC surgery, hemodynamic measurements, and histological analyses were performed as described (5). Briefly, pressure overload was evoked by the surgical TAC. TAC was performed on 6-week-old male C57BL6j mice. A mini-osmotic pump (Alzet) filled with polyethylene glycol or Pyr3 (0.1 mg/kg/day) was implanted intraperitoneally in mice 3 d before 1 week of TAC. In the case of 6 weeks of TAC, Pyr3 was treated 3 d after TAC. Six weeks after TAC operation, transthoracic echocardiography was performed using ALOKA ultrasonic image analyzing system (SSD-5500) equipped with 7.5 MHz imaging transducer. Hemodynamic measurements were taken by inserting a micromanometer catheter (Millar 1.4F, SPR 671, Millar Instruments) from the right common carotid artery into the aorta and then the left ventricle. To calculate pressure gradient, distal arterial pressure was measured using tail-cuff detection system (Softron, BP-98A). After heart weight was measured, total RNA was isolated. The quantitative measurement of ANP mRNA expression was performed by real time RT-PCR. Primers and probe for mouse ANP mRNA are as follow: forward primer, 5'-CATCACCTGGGCTTCTTCCT-3'; reverse primer, 5'-TGGGCTCCAATCCTGTCAATC-3'; TaqMan[®] probe, 5'-ATTTCAAGAACCTGCTAGACCACCTGGA-3'. All mouse protocols were approved by the guidance of Kyushu University.

Immunoprecipitation. PLC γ 1 cDNA according to NM_002660 was isolated from human testis cDNA library (CLONTECH). PLC γ 1-FLAG was constructed as

PLC γ 2-FLAG (1). Forty-eight h after transfection with PLC γ 1-FLAG or PLC γ 2-FLAG, HEK293 cells were lysed in NP-40 lysis buffer (137 mM NaCl, 20 mM Tris-HCl, pH 8.0, 1% NP-40, 1 mM PMSF, 20 μ g/ml leupeptin, 0.1 μ g/ml aprotinin, and 1 mM PMSF). PLC γ 2-FLAG or PLC γ 1-FLAG was immunoprecipitated in NP-40 lysis buffer with 2 μ l of anti-FLAG M2 antibody (Sigma) rotating 6 h at 4 °C. Thirty μ l of protein A-agarose beads (Amersham Pharmacia) were then added to the samples, and rocked for further 2 h at 4°C on a slow rotator. The immune complexes were washed three times with the NP-40 lysis buffer, and resuspended in 50 μ l of the SDS sample buffer. The protein samples were fractionated by 8% SDS-PAGE and electrotransferred onto a nitrocellulose membrane. The blots were incubated with anti-TRPC3 antibody (1).

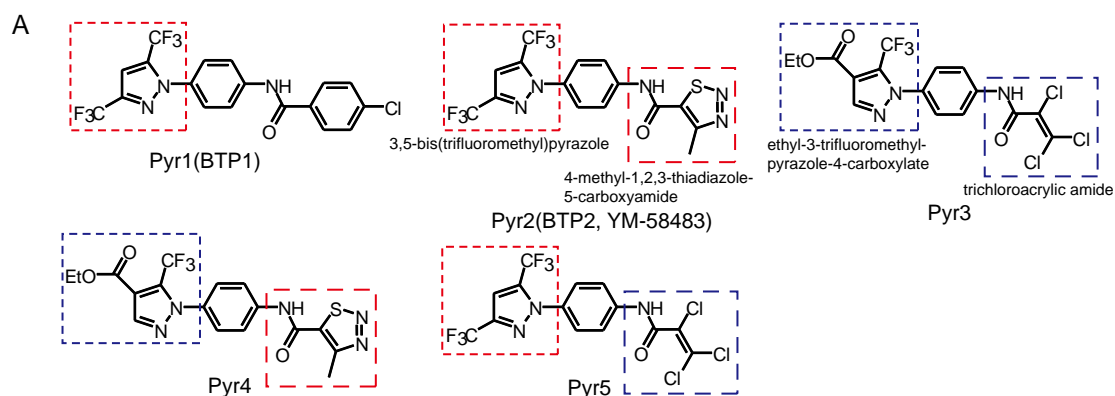
NFAT activity in DT40 cells. NFAT activity was quantitated with 1420 ARVOSx (Wallac) using NFAT luciferase genes and the Dual-LuciferaseTM assay system (Promega) as described (6). Luciferase activity was determined in triplicate for each experimental condition.

Statistical Analysis. All data are expressed as means \pm SEM. The data were accumulated under each condition from at least three independent experiments. The *P* values are the results of Student's *t*-tests. One-way analysis of variance followed by Student-Newman-Keuls procedure was performed in comparison with more than two groups. Linear regression analyses were run for Pyr3-treated and vehicle-treated groups separately. Analysis of relations between heart weight-to-tibia ratio or fractional shortening and systolic pressure gradient for both groups were carried out as

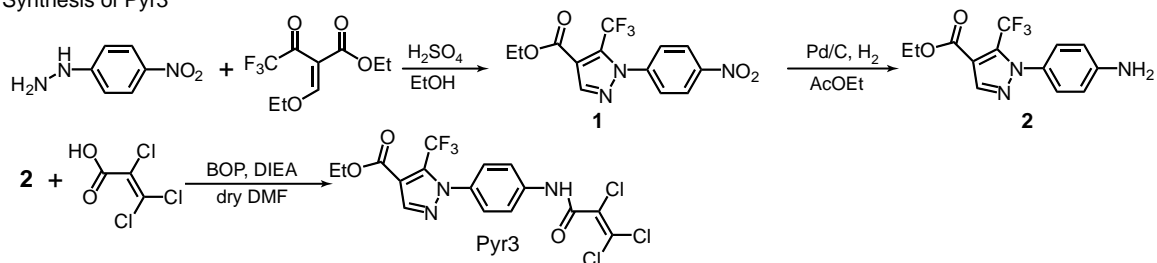
described (7).

SI References

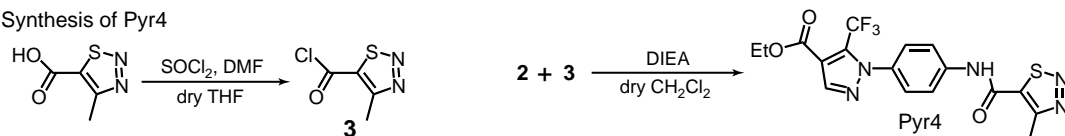
1. Nishida M, *et al.* (2003) Amplification of receptor signalling by Ca²⁺ entry-mediated translocation and activation of PLC γ 2 in B lymphocytes. *EMBO J* 22:4677–4688.
2. Okada T, *et al.* (1999) Molecular and functional characterization of a novel mouse transient receptor potential protein homologue TRP7. *J Biol Chem* 274:27359–27370.
3. Mio K, Ogura T, Hara Y, Mori Y, Sato C (2005) The non-selective cation-permeable channel TRPC3 is a tetrahedron with a cap on the large cytoplasmic end. *Biochem Biophys Res Commun* 333:768–777.
4. Onohara N, *et al.* (2006) TRPC3 and TRPC6 are essential for angiotensin II-induced cardiac hypertrophy. *EMBO J* 25:5305–5316.
5. Nishida M, *et al.* (2008) P2Y₆ receptor-G $\alpha_{12/13}$ signalling in cardiomyocytes triggers pressure overload-induced cardiac fibrosis. *EMBO J* 27:3104–3115.
6. Sugawara H, Kurosaki M, Takata M, Kurosaki T (1997) Genetic evidence for involvement of type 1, type 2 and type 3 inositol 1,4,5-trisphosphate receptors in signal transduction through the B-cell antigen receptor. *EMBO J* 16:3078–3088.
7. Rockman HA, Wachhorst SP, Mao L, Ross J Jr (1994) Ang II receptor blockade prevents ventricular hypertrophy and ANF gene expression with pressure overload in mice. *Am J Physiol* 266: H2468–H2475.



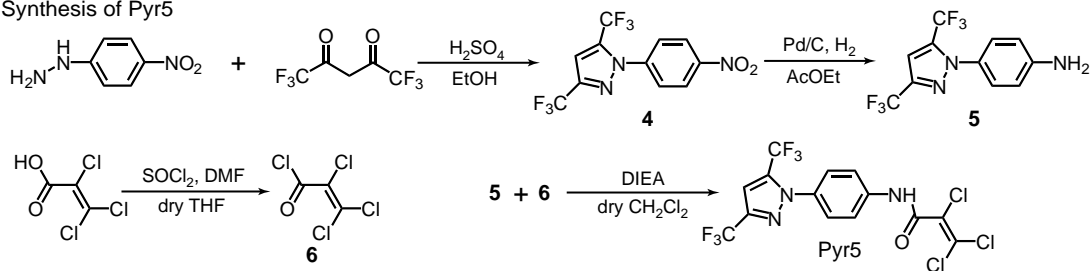
B Synthesis of Pyr3



C Synthesis of Pyr4



D Synthesis of Pyr5



E Synthesis of Pyr-PP

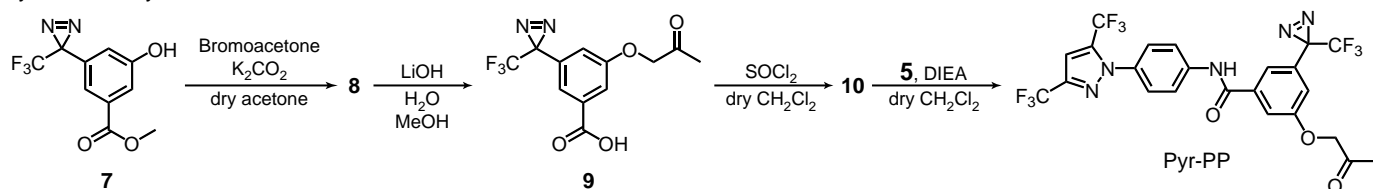


Figure S1. Chemical structures and synthetic schemes of pyrazole compounds. (A) Chemical structures of Pyr1, Pyr2, Pyr3, Pyr4, and Pyr5. (B–E) Synthetic schemes of Pyr3 in B, Pyr4 in C, Pyr5 in D, and Pyr-PP in E. Pyr-PP is designed based on the chemical structure of Pyr2.

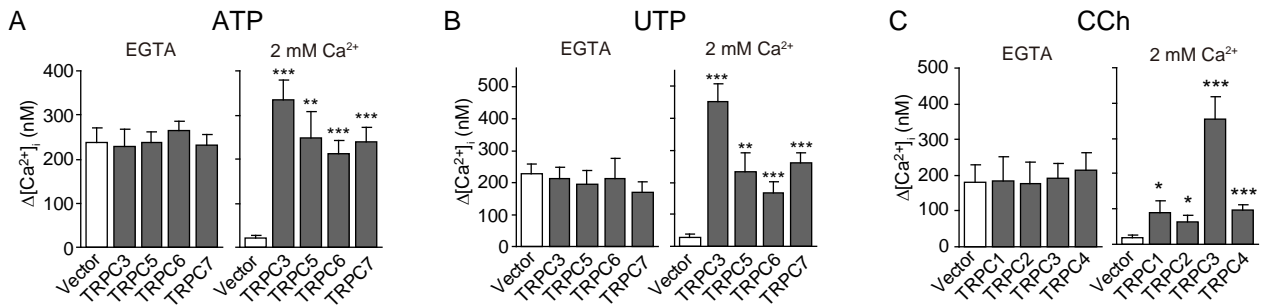


Figure S2. Comparisons with vector-transfected control cells support receptor-induced activation of Ca²⁺ influx through respective TRPCs in transfected HEK293 cells. Peak [Ca²⁺]_i rises in Ca²⁺-free, 0.5 mM EGTA- (*Left*) or 2 mM Ca²⁺-containing solution (*Right*) under constant stimulation with 100 μM ATP (*A*), UTP (*B*), or CCh (*C*) obtained by similar procedures as those described in Fig. 1B (n = 24–33). *P < 0.05, **P < 0.01, and ***P < 0.001 vs vector.

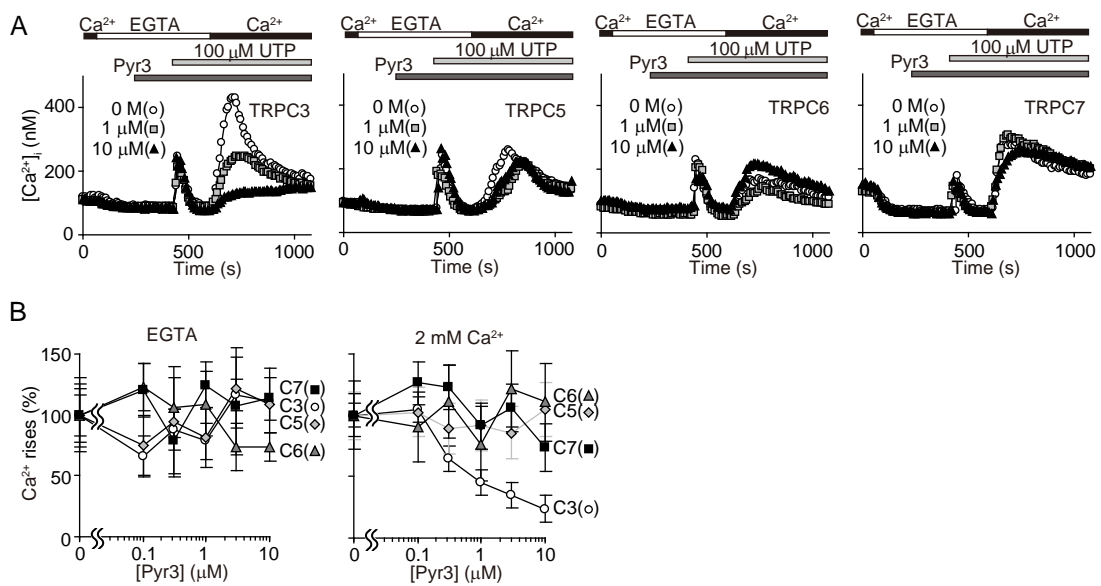


Figure S3. Concentration-dependent inhibitory action of Pyr3 on UTP stimulation-induced Ca²⁺ influx via TRPCs. (A) Average time courses of Ca²⁺ responses induced by 100 μM UTP with Pyr3 at indicated concentrations in TRPC-transfected HEK293 cells. (B) Percentage peak [Ca²⁺]_i rises in Ca²⁺-free, 0.5 mM EGTA- (Left) or 2 mM Ca²⁺-containing external solution (Right) compared to control responses without Pyr3 (n = 24–47).

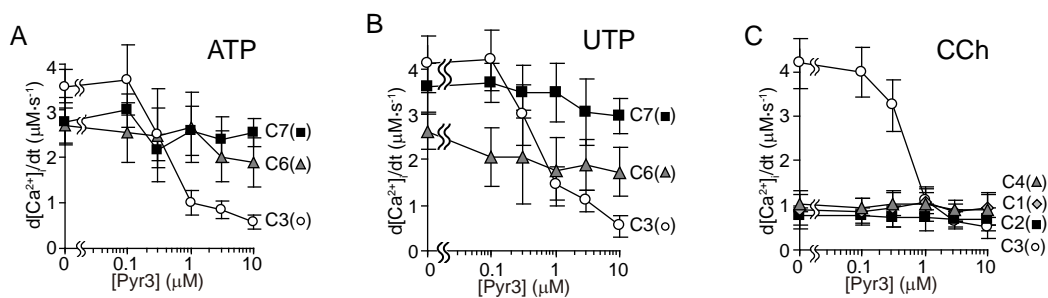


Figure S4. Pyr3 attenuates initial rates of TRPC-mediated Ca²⁺ influx. (A) Effects of Pyr3 on ATP-induced Ca²⁺ influx rates in TRPC3-, TRPC6-, TRPC7-transfected HEK293 cells. (B) Effects of Pyr3 on UTP-induced Ca²⁺ influx rates in TRPC3-, TRPC6-, TRPC7-transfected HEK293 cells. (C) Effects of Pyr3 on CCh-induced Ca²⁺ influx rates in TRPC1-, TRPC2-, TRPC3-, TRPC4-transfected HEK293T cells. With regard to TRPC5, Ca²⁺ entry rate is not determined, because TRPC5-mediated Ca²⁺ responses frequently show variable time lags after readdition of extracellular Ca²⁺ in contrast to Ca²⁺ responses induced by other TRPCs (ref. Ordaz B, *et al.* (2005) Calmodulin and calcium interplay in the modulation of TRPC5 channel activity. *J Biol Chem* 280:30788–30796.).

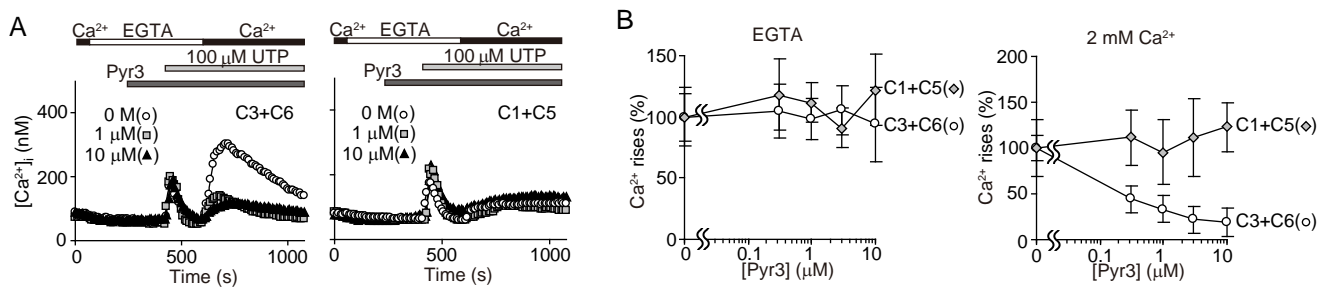


Figure S5. Inhibitory action of Pyr3 on UTP stimulation-induced Ca²⁺ influx in HEK293 cells co-expressing TRPC subtypes. (A) Average time courses of Ca²⁺ responses induced by 100 μM UTP with Pyr3 at indicated concentrations in HEK293 cells co-transfected with TRPC3 and TRPC6 (Left), or with TRPC1 and TRPC5 (Right). (B) Percentage peak [Ca²⁺]_i rises in Ca²⁺-free, 0.5 mM EGTA- (Left) or 2 mM Ca²⁺-containing external solution (Right) compared to control responses without Pyr3 (n = 23–37).

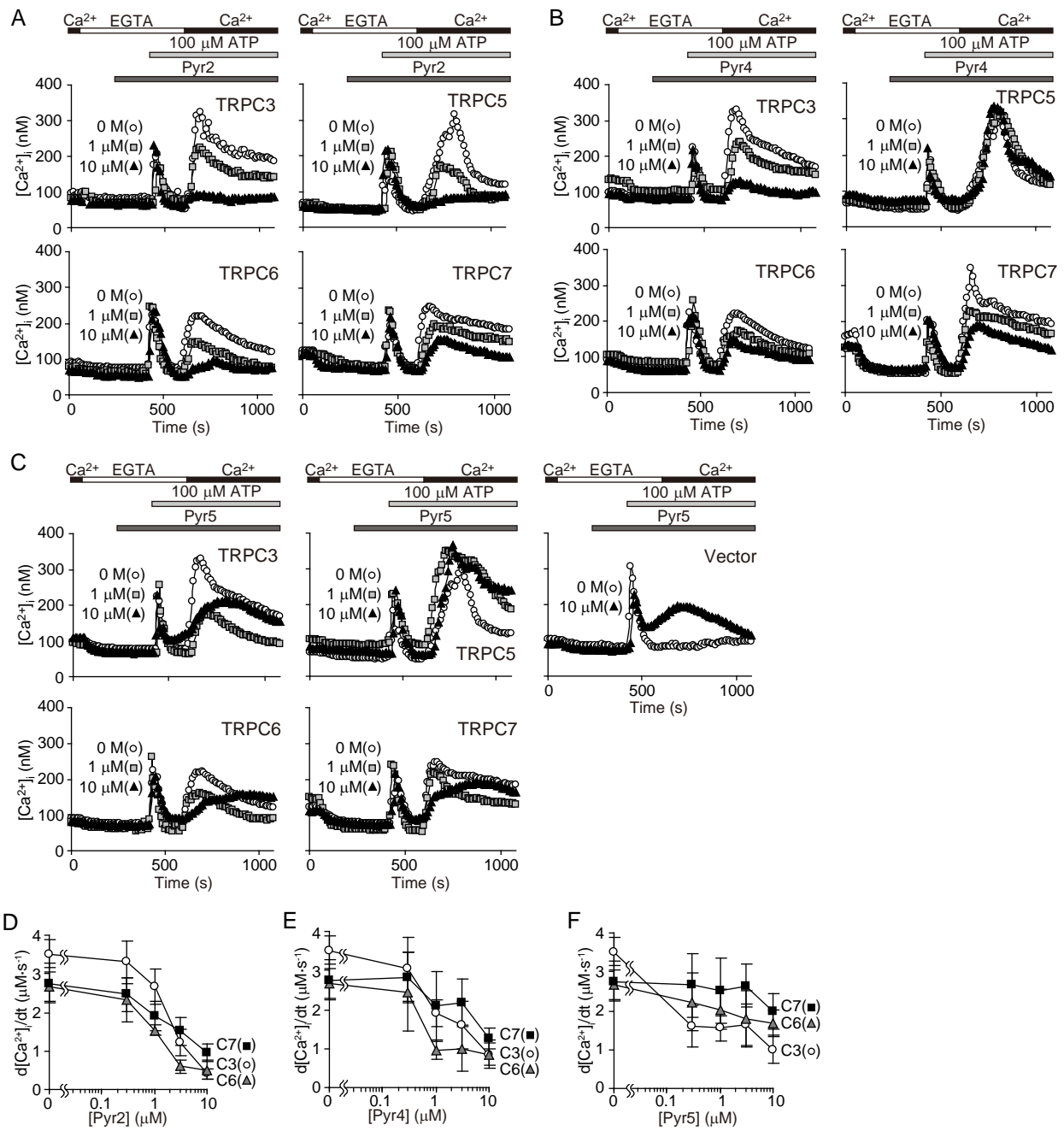


Figure S6. Time courses of ATP receptor-induced Ca^{2+} responses in the presence of Pyr2 and chimeric derivatives. (A–C) Concentration-dependent inhibitory action of Pyr2 (A), Pyr4 (B), or Pyr5 (C) on Ca^{2+} influx induced by 100 μM ATP among TRPCs. In C, 10 μM Pyr5 enhances Ca^{2+} responses in vector-transfected control HEK293 cells. (D–F) Effects of Pyr2 (D), Pyr4 (E), or Pyr5 (F) on Ca^{2+} influx rates in TRPC3-, TRPC6-, TRPC7-transfected HEK293 cells.

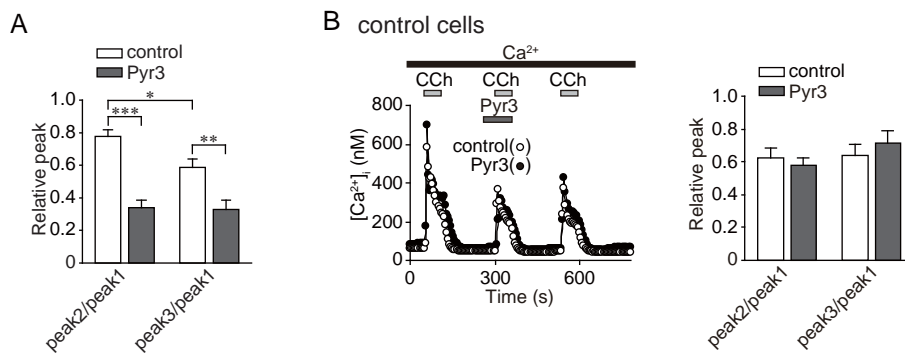


Figure S7. The recovery of Pyr3 from blockade is a slow process. (A) TRPC3 currents are induced by 100 μ M CCh using the testing paradigm depicted in Fig. 3B. The amplitude of the second response and third response are normalized to that of the first response (peak2/peak1 and peak3/peak1, respectively) ($n = 5$). (B) Ca^{2+} responses induced by repeated CCh stimulation of endogenous mACh receptors are unaffected by Pyr3 in control cells. (Left) Average time course of Ca^{2+} responses induced by 60 μ M CCh in HEK293 cells (open circle). Three μ M Pyr3 is added 1 min before second stimulation of CCh into the external solution (closed circle). (Right) The peak $[Ca^{2+}]_i$ rises of the second response and third response are normalized to that of the first response (peak2/peak1 and peak3/peak1, respectively). * $P < 0.05$, ** $P < 0.01$, and *** $P < 0.001$.

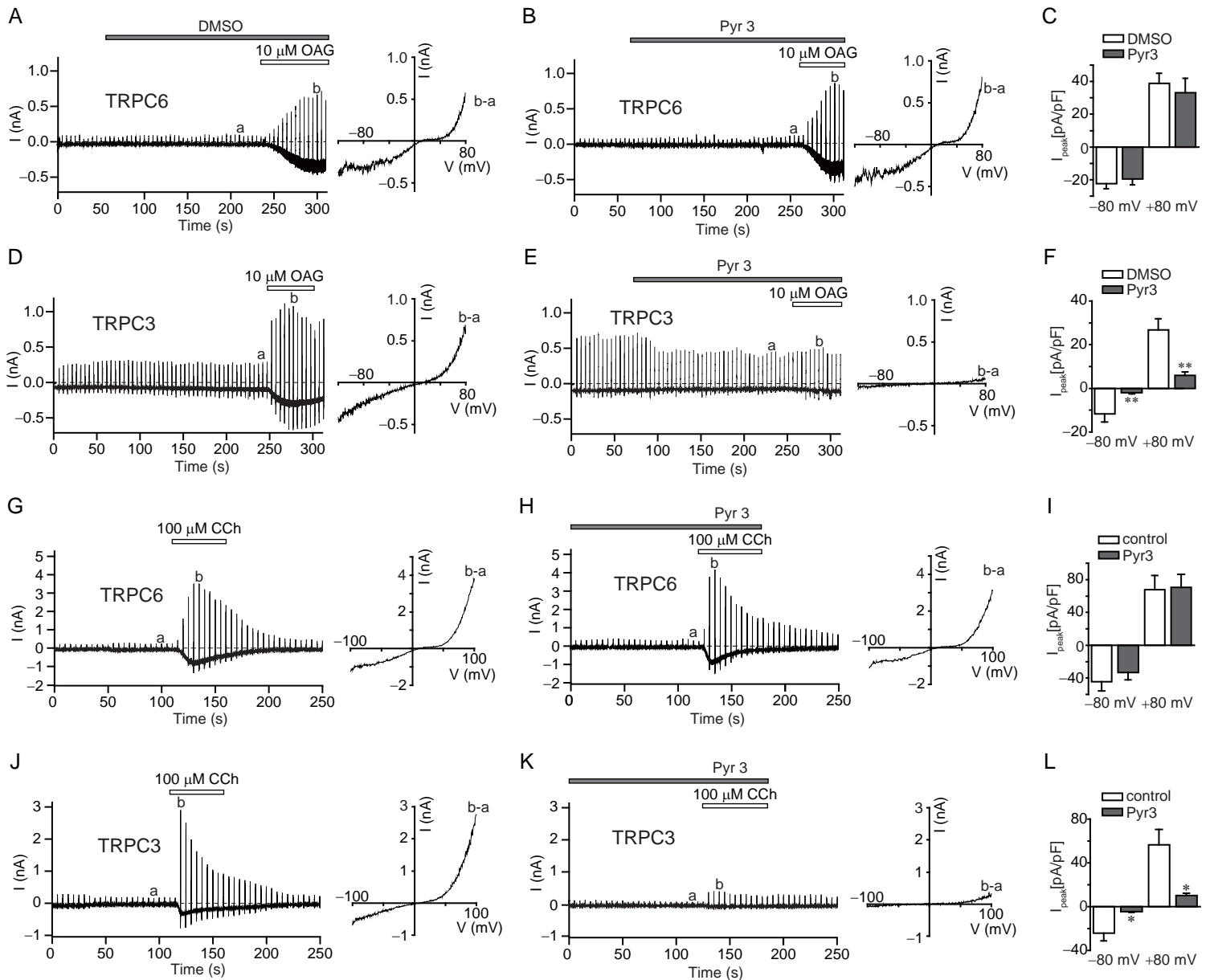


Figure S8. TRPC6 currents are unaffected by Pyr3 in contrast to TRPC3 currents. (A–F) OAG-induced TRPC6 currents are unaffected by Pyr3 in contrast to OAG-induced TRPC3 currents. (A and B) Ionic currents induced by 10 μM OAG at a holding potential -60 mV in TRPC6-transfected HEK293 cells. Current fluctuations evoked by voltage-ramps from -120 mV to $+80$ mV are also shown. 0.1% DMSO (A) or 3 μM Pyr3 (B) is added 3 min before the addition of OAG to the external solution (Left). I - V relationships of OAG-induced currents obtained by subtracting the currents evoked by the voltage-ramps before activation of channels (current traces a) from those after activation (current traces b) (Right). (C) Average densities of OAG-induced TRPC6 currents at -80 mV or $+80$ mV. The same sets of experiments as in (A), (B), and (C) are performed for TRPC3 in (D), (E), and (F), respectively. $**P < 0.01$ vs DMSO. (G–L) CCh-induced TRPC6 currents are unaffected by Pyr3 in contrast to CCh-induced TRPC3 currents. (G and H) Ionic currents induced by 100 μM CCh at a holding potential of -50 mV in TRPC6-transfected HEK293 cells. Current fluctuations evoked by voltage-ramps from -100 mV to $+100$ mV are also shown (Left). I - V relationships of CCh-induced currents obtained by subtracting the currents evoked by the voltage-ramps before activation of channels (current traces a) from those after activation (current traces b) (Right). (H) Three μM Pyr3 is added 3 min before the addition of CCh to the external solution. (I) Average densities of CCh-induced TRPC6 currents at -80 mV or $+80$ mV. The same sets of experiments as in (G), (H), and (I) are performed for TRPC3 in (J), (K), and (L), respectively. $*P < 0.05$ vs control.

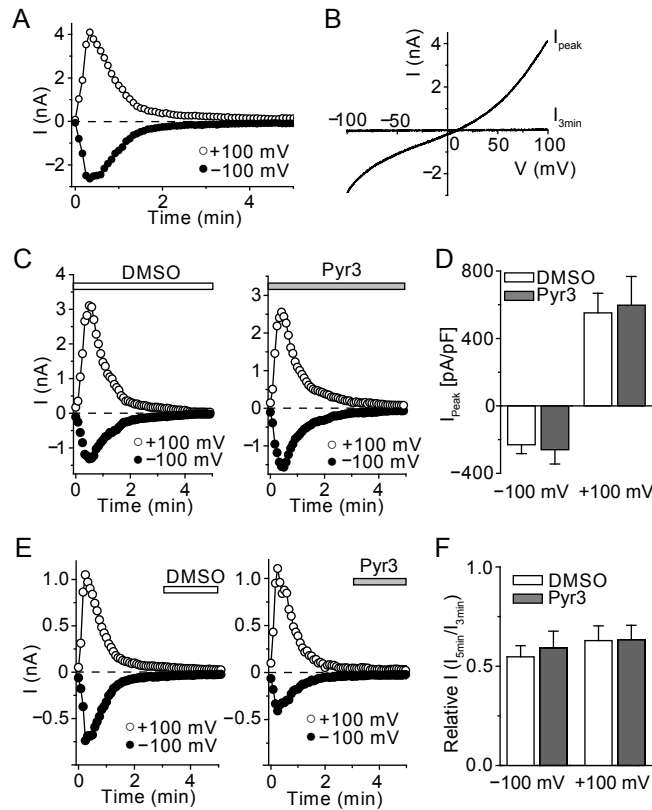


Figure S9. Intracellular Ca^{2+} -activated TRPM4 current is not suppressed by extracellular application of Pyr3. (A) Representative inward and outward currents induced by $100 \mu\text{M}$ intracellular Ca^{2+} at -100 and $+100$ mV, respectively, in TRPM4b-transfected HEK293 cells. Immediately following establishment of the whole-cell configuration, voltage ramps from -100 to $+100$ mV are delivered from a holding potential of 0 mV. (B) I - V relationships of intracellular Ca^{2+} -induced whole cell currents obtained at the peak of current and at 3 min after whole-cell establishment. (C–F) Lack of Pyr3 effect on TRPM4 channels. (C and E) Representative inward and outward currents induced by $100 \mu\text{M}$ intracellular Ca^{2+} at -100 and $+100$ mV, respectively, in TRPM4b-transfected HEK293 cells treated with DMSO or Pyr3 ($3 \mu\text{M}$). In C, treatments are started immediately prior to the whole-cell mode recording, while in E, treatments are started 3 min after the establishment of whole-cell mode. (D) Average densities of currents at -100 and $+100$ mV with and without $3 \mu\text{M}$ Pyr3 in TRPM4b-transfected cells ($n = 6$ – 7), as C. (F) Relative currents at -100 and $+100$ mV obtained 5 min (after treatment) and 3 min (before treatment) after the establishment of whole-cell mode in the treatment ($n = 8$ – 15) in TRPM4b-transfected cells.

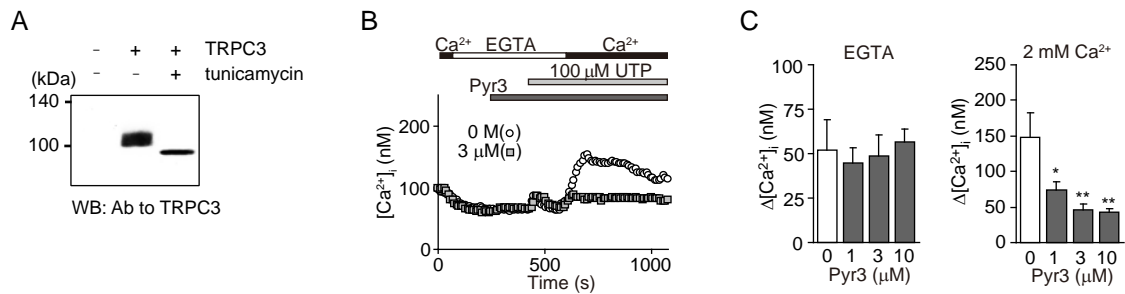


Figure S10. Pyrene sensitivity is unaffected by inhibition of glycosylation of the TRPC3 protein. (A) WB using anti-TRPC3 antibody shows that application of 1 μg/ml tunicamycin in HEK293 cells inhibits glycosylation of TRPC3 proteins. Cells are incubated with tunicamycin from 3 h after cDNA transfection till they are harvested for WB analysis. (B and C) Concentration-dependent inhibitory action of Pyrene on UTP stimulation-induced Ca²⁺ influx via TRPC3 in the presence of tunicamycin. (B) Average time courses of Ca²⁺ responses induced by 100 μM UTP with Pyrene at indicated concentrations in TRPC3-transfected HEK293 cells. (C) Percentage peak [Ca²⁺]_i rises in Ca²⁺-free, 0.5 mM EGTA- (Left) or 2 mM Ca²⁺-containing external solution (Right) compared to control responses without Pyrene (n = 20–35). *P < 0.05 and **P < 0.01 vs 0 μM Pyrene.

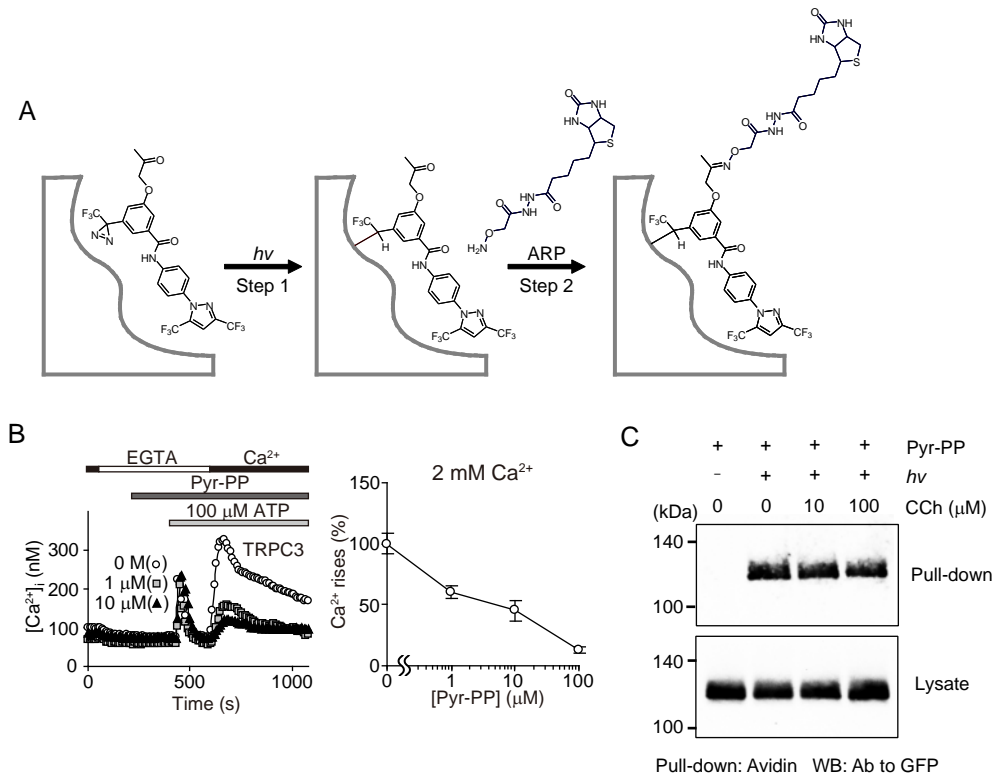


Figure S11. The P-PALM method using Pyr-PP. (A) Schematic representation of the P-PALM method using Pyr-PP. The photoreaction forms a covalent bond between the ligand and target protein (step1), and the consecutive oxime bond formation between the ketone group and ARP allows collections of labelled proteins using biotin-avidin binding (step2). (B) Inhibitory action of Pyr-PP on ATP receptor-activated Ca²⁺ influx via TRPC3. Average time courses of Ca²⁺ responses induced by stimulation with 100 μM ATP in TRPC3-transfected HEK293 cells (*Left*). Percentage peak [Ca²⁺]_i rises in 2 mM Ca²⁺-containing solution compared to control responses without Pyr3 (*Right*, n = 21–33). IC₅₀ value of Pyr-PP is around 2 μM. (C) CCh fails to influence photo-labeling of TRPC3 with Pyr-PP. Photo-labeling is performed immediately after addition of each concentration of CCh in HBS solution. After P-PALM, TRPC3-GFP proteins are detected with anti-GFP antibody by WB in avidin pull-down samples.

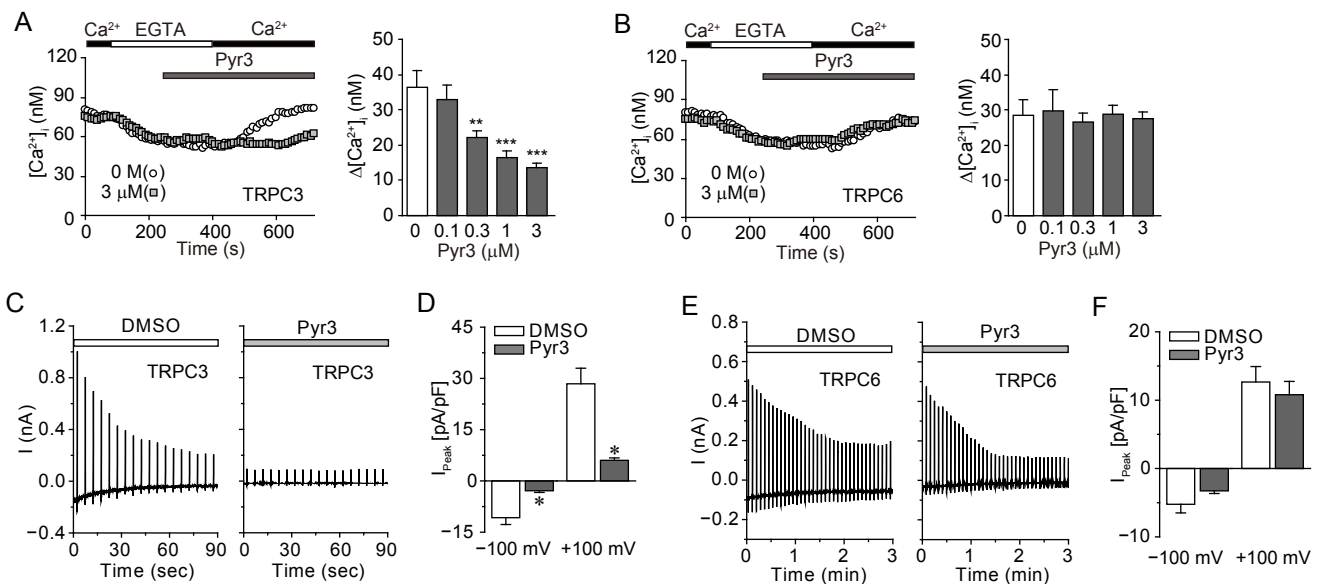


Figure S12. Constitutive activity of TRPC3 but not that of TRPC6 is inhibited by Pyr3. (*A* and *B*) Effects of Pyr3 on constitutively activated Ca^{2+} influx via TRPC3 (*A*) or TRPC6 (*B*) in HEK293 cells. Average time courses of Ca^{2+} responses with Pyr3 at indicated concentrations in TRPC-transfected HEK293 cells (*Left*). Peak $[\text{Ca}^{2+}]_i$ rises after readministration of 2 mM Ca^{2+} -containing external solution (*Right*) ($n = 25\text{--}38$). $**P < 0.01$ and $***P < 0.001$ vs 0 μM Pyr3. (*C*–*F*) Constitutively activated currents of TRPC3 but not those of TRPC6 are suppressed by extracellular application of Pyr3. (*C* and *E*) Traces of whole-cell ionic currents at a holding potential of -50 mV in TRPC3- or TRPC6-transfected HEK293 cells. Current fluctuations evoked by voltage-ramps from -100 mV to $+100$ mV are also shown. (*D* and *F*) Average current densities at -100 mV and $+100$ mV of the 1st voltage-ramp in the presence or absence of 3 μM Pyr3 in the external solution in HEK293 cells transfected with TRPC3 ($n = 8\text{--}27$) or TRPC6 ($n = 7\text{--}18$). $*P < 0.05$ vs DMSO.

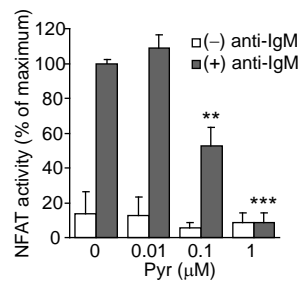


Figure S13. Effects of Pyr3 on NFAT activity in DT40 cells. DT40 cells transfected with the NFAT luciferase gene are analyzed as described in *SI Methods*. ** $P < 0.01$ and *** $P < 0.001$ vs 0 μM Pyr3.

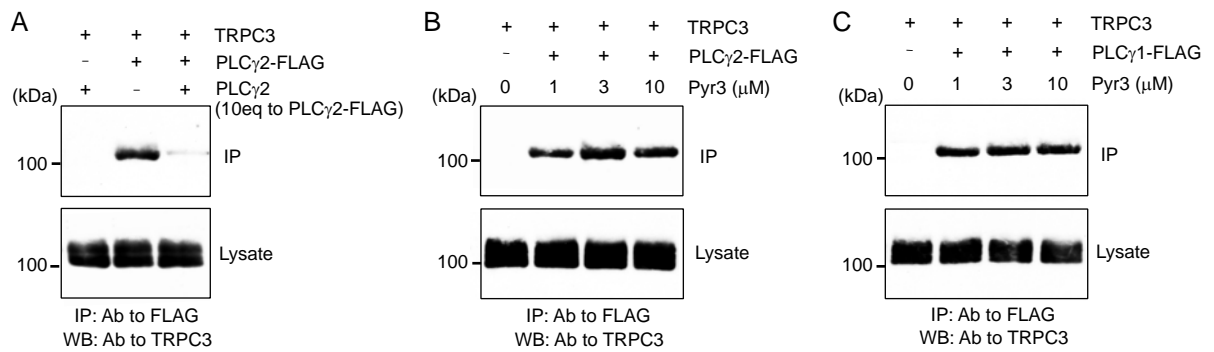


Figure S14. The interaction of PLC γ s with TRPC3 is unaffected by Pyr3. (A–C) Co-immunoprecipitation of TRPC3 with PLC γ 2-FLAG (B) or PLC γ 1-FLAG (C) in the presence of Pyr3 at indicated concentrations. As a control experiment, disruption of the interaction between PLC γ 2-FLAG and TRPC3 by PLC γ 2 is shown in A.

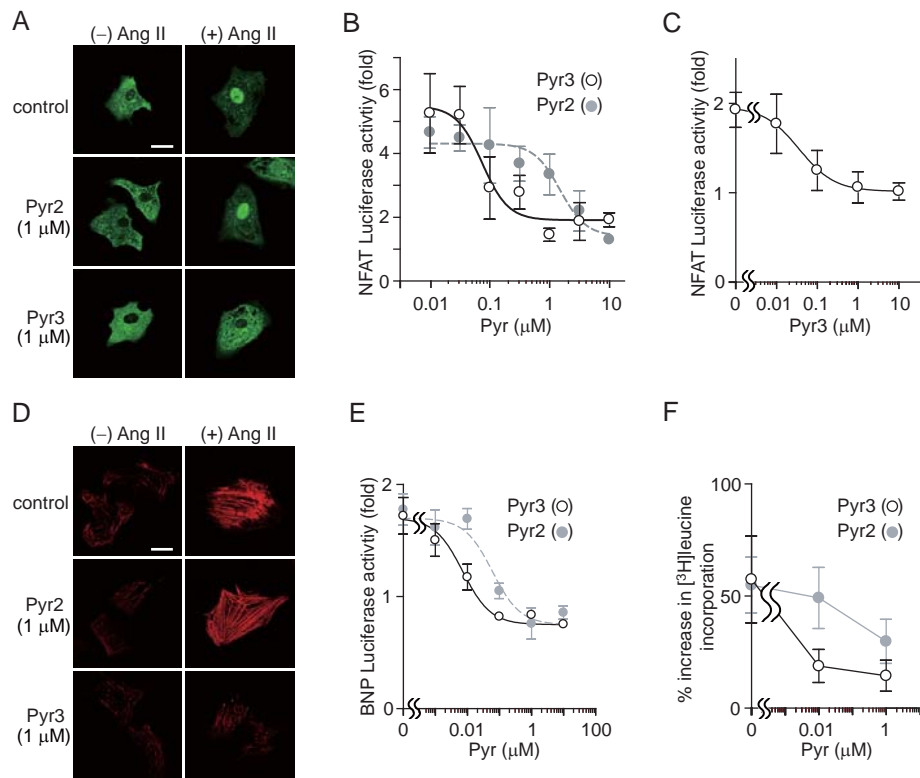


Figure S15. Pyr3 potently suppresses hypertrophic responses in rat neonatal cardiomyocytes. (A–C) Effects of Pyr2 or Pyr3 on NFAT activation induced by Ang II or mechanical stretch in rat neonatal cardiomyocytes. (A) Confocal images of the localization of GFP-NFAT proteins. Cells are treated with Pyr2 or Pyr3 for 20 min prior to the stimulation with Ang II (100 nM) for 30 min. The bar indicates 20 μ m. (B and C) Concentration-dependent inhibitory effects of Pyr2 or Pyr3 on the increase in NFAT-luciferase activity induced by Ang II (B), and by mechanical stretch (C). Cells are treated with Pyr2 or Pyr3 for 20 min prior to the stimulation with Ang II (100 nM) or mechanical stretch by 20% for 6 h. (D–F) Effects of Pyr2 or Pyr3 on the Ang II-induced actin reorganization (D), and on increases in BNP-luciferase activity (E) and incorporation of [³H]leucine (F). Cells are treated with Pyr2 or Pyr3 for 20 min prior to the stimulation with Ang II (100 nM) for 48 h (D and E) or 6 h (F). The bar indicates 20 μ m.

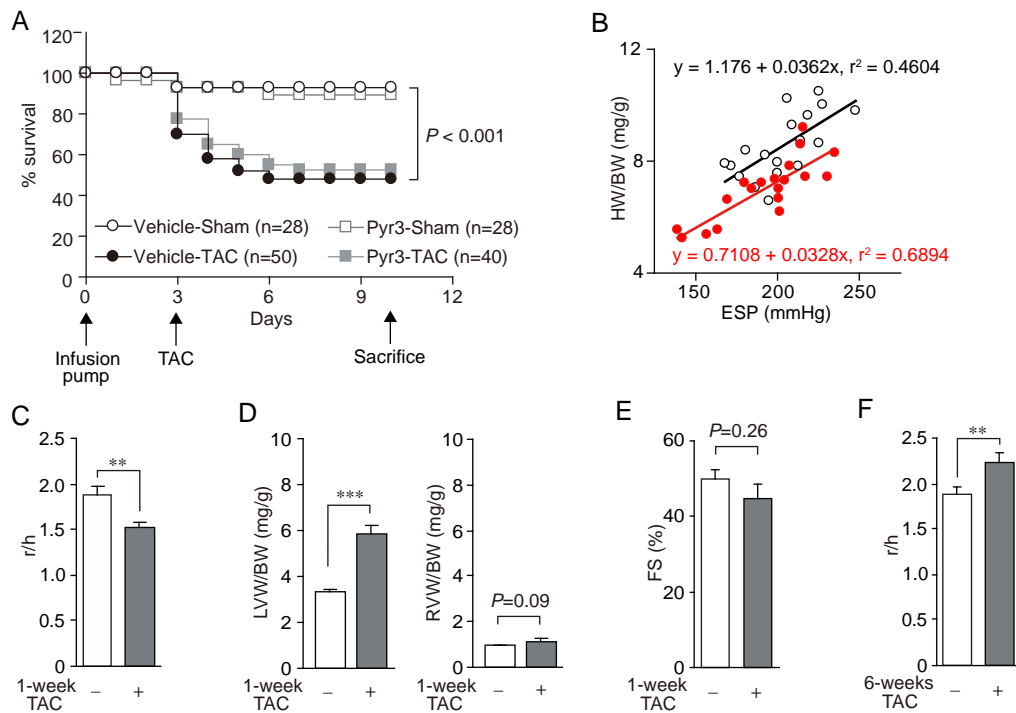


Figure S16. Effects of Pyr3 on TAC-induced hypertrophy. (A–E) Effects of Pyr3 on concentric hypertrophy. (A) Surgical stress and pressure overload are equally loaded on both groups TAC-operated with and without Pyr3. Kaplan-Meier survival analysis. Percentages of surviving vehicle-sham (n = 28), vehicle-TAC (n = 50), Pyr3-sham (n = 28) and Pyr3-TAC (n = 40) are plotted. Between-group difference is analyzed by the log-rank test. (B) Scattergram of HW/BW ratio vs ESP of TAC mice with (red; n = 19) and without (black; n = 18) treatment with Pyr3. Pyr3 significantly shifts relationships downward in HW/BW ($P < 0.001$). HW/BW, ratio of heart weight to body weight. (C) Ratio of internal ventricular radius at end diastole (r) to ventricular wall thickness (h) induced by 1 week of TAC. Wall thickness is measured using echocardiography. (D) TAC-induced increases of left ventricle and right ventricle weight. LVW/BW, ratio of left ventricle weight to body weight; RVW/BW, right ventricle weight to body weight. (E) Deterioration of fractional shortening (FS) is not observed by 1 week of TAC. (F) Increase of r/h ratio induced by 6 weeks of TAC demonstrating dilated hypertrophy. ** $P < 0.01$ and *** $P < 0.001$.

Table S1 Anatomic findings and hemodynamic parameters in vehicle- or Pyr3-treated mice at 1 week after TAC operation to induce concentric hypertrophy.

Variable (n = 12–24)	Vehicle		Pyr3	
	Sham	TAC	Sham	TAC
BW (g)	21.7 ± 0.4	20.5 ± 0.4	21.6 ± 0.5	20.3 ± 0.3
HW (mg)	100.6 ± 2.0	154.6 ± 3.8 ^{***}	100.5 ± 2.1	123.9 ± 2.9 ^{***###}
HW/BW (mg/g)	4.63 ± 0.05	7.56 ± 0.18 ^{***}	4.66 ± 0.05	6.10 ± 0.13 ^{***###}
LuW/BW (mg/g)	6.44 ± 0.17	7.91 ± 0.54 [*]	6.30 ± 0.08	6.64 ± 0.20 [#]
LiW/BW (mg/g)	52.78 ± 1.11	52.98 ± 2.12	53.11 ± 1.34	54.26 ± 1.20
HR (beats/min)	499 ± 2	493 ± 3	501 ± 7	498 ± 2
ESP (mmHg)	110 ± 1	206 ± 4 ^{**}	110 ± 2	192 ± 6 ^{**}
EDP (mmHg)	3.0 ± 0.3	8.3 ± 0.7 ^{**}	2.9 ± 0.4	5.4 ± 0.4 ^{###}
dP/dt _{max} (mmHg/s)	10203 ± 335	9365 ± 183	9818 ± 306	9791 ± 216
dP/dt _{min} (mmHg/s)	6839 ± 153	8333 ± 295 ^{**}	7059 ± 197	8598 ± 291 ^{**}
τ (msec)	10.4 ± 0.2	12.7 ± 0.5 ^{**}	10.5 ± 0.4	10.9 ± 0.3 [#]

BW, body weight; HW, heart weight; HW/BW, ratio of heart to body weight, LuW/BW, ratio of lung to body weight; LiW/BW, ratio of liver to body weight; HR, heart rate; ESP, left ventricular end-systolic pressure; EDP, left ventricular end-diastolic pressure; dP/dt_{max}, maximum rate of developed left ventricular pressure; dP/dt_{min}, minimum rate of developed left ventricular pressure; τ, time constant of isovolumic relaxation. ^{*}P < 0.05, ^{**}P < 0.01, and ^{***}P < 0.001 vs Sham. [#]P < 0.05, ^{##}P < 0.01, and ^{###}P < 0.001 vs Vehicle TAC.

Table S2 Anatomic findings and hemodynamic parameters in vehicle- or Pyr3-treated mice at 6 weeks after TAC operation to induce dilated hypertrophy.

Variable (n = 9–12)	Vehicle		Pyr3	
	Sham	TAC	Sham	TAC
BW (g)	24.2 ± 0.42	24.6 ± 0.8	24.0 ± 0.29	24.4 ± 0.26
HW (mg)	105.8 ± 3.1	212.3 ± 11.3 ^{***}	104.5 ± 2	185.4 ± 6.4 ^{***#}
HW/BW (mg/g)	4.38 ± 0.08	8.75 ± 0.64 ^{***}	4.36 ± 0.09	7.47 ± 0.21 ^{***#}
LuW/BW (mg/g)	5.37 ± 0.09	10.13 ± 1.85 [*]	5.48 ± 0.14	6.54 ± 0.45 [#]
LiW/BW (mg/g)	48.46 ± 0.83	47.92 ± 2.39	49.82 ± 1.75	45.28 ± 1.23
HR (beats/min)	499 ± 3	498 ± 8	493 ± 4	501 ± 3
ESP (mmHg)	114 ± 3	227 ± 8 ^{***}	120 ± 2	228 ± 9 ^{***}
EDP (mmHg)	3.0 ± 0.2	9.8 ± 0.8 ^{***}	3.4 ± 0.6	5.4 ± 0.5 ^{####}
dP/dt _{max} (mmHg/s)	10340 ± 425	10010 ± 370	10650 ± 554	9451 ± 740
dP/dt _{min} (mmHg/s)	7175 ± 223	8405 ± 448	7392 ± 198	8608 ± 702
τ (msec)	10.34 ± 0.19	13.93 ± 0.89 ^{***}	10.42 ± 0.3	11.16 ± 0.46 ^{#####}
FS (%)	68.29 ± 2.36	28.89 ± 2.16 ^{***}	70.29 ± 0.99	49.11 ± 3.16 ^{#####}

P* < 0.05 and **P* < 0.001 vs Sham. #*P* < 0.05 and ####*P* < 0.001 vs Vehicle TAC.